ELSEVIER

Journal of Molecular Catalysis A: Chemical 161 (2000) 191–204

JOURNAL OF MOLECULAR CATALYSIS A: CHEMICAL

www.elsevier.com/locate/molcata

Investigation of the state of copper in supported copper–titanium oxide catalysts

O.V. Komova, A.V. Simakov *, V.A. Rogov, D.I. Kochubei, G.V. Odegova, V.V. Kriventsov, E.A. Paukshtis, V.A. Ushakov, N.N. Sazonova, T.A. Nikoro

Boreskov Institute of Catalysis, Pr. Akademika Lavrentieva 5, Novosibirsk 630090, Russia

Received 22 December 1999; received in revised form 31 May 2000; accepted 16 June 2000

Abstract

Supported copper–titanium oxide catalysts have been studied by IR spectroscopy, XRD, UV–VIS diffuse reflectance spectroscopy, ESR, TPR with hydrogen and EXAFS. Different states of Cu^{2+} ions have been found on the surface of TiO_2. The ratio between these states depends on the copper concentration and catalyst preparation method. Chain structures are formed due to the interaction of Cu^{2+} ions with TiO_2. Their concentration and geometry of their nearest oxygen environment are determined by the structure of anatase faces. Some of these surface-stabilized Cu^{2+} ions are nucleation centers of oxide clusters. A noticeable growth of bulk CuO phase is observed after the completion of the formation of chain structures and oxide clusters. A quantitative estimation of the concentration of these copper forms in the catalysts is reported. For supported copper–titanium oxide catalysts, chain forms of Cu^{2+} ions are shown to be the most active forms of copper in NO SCR with ammonia and methane oxidation.

Keywords: Copper states; Titania; CH_4 oxidation; SCR with ammonia

1. Introduction

Copper–titanium oxide (Cu–Ti–O) catalysts are active in deep oxidation of CO and hydrocarbons [1,2] and selective catalytic reduction (SCR) of NO [3–6]. The prospects of the application of these catalysts for complex purification of flue gases from NO, CO and harmful organic compounds are discussed in [7]. The activity of this catalytic system in deep oxidation reactions has been shown to depend on the surface copper concentration [1,2]. Nanosize forms of Cu^{2+} ions are claimed to have the main contribution to the activity in comparison with bulk CuO phase. Similar conclusions have been obtained during investigation of the activity of these catalysts in the NO SCR with ammonia [3].

Various physicochemical methods have been used for investigation of the state of copper ions in supported Cu–Ti–O catalysts: ESR, XRD, IR spec-

* Corresponding author. Tel.: +7-383-234-1681; fax: +7-383-234-3056.

E-mail address: asimakov@catalysis.nsk.su (A.V. Simakov).

1381-1169/00/$ - see front matter
PII: S1381-1169(00)00342-3

troscopy, UV–VIS diffuse reflectance spectroscopy, XPS, TPR with H_2. It has been shown by XRD and ESR [8] that a low-concentration solid substitution solution of copper in TiO_2, Cu^{2+} ions stabilized on the surface of titania and CuO phase are formed in this system. According to the data obtained by IR spectroscopy of probe molecules (CO), ESR and UV–VIS diffuse reflectance spectroscopy [9–11], stabilization of copper ions is due to their interaction with basic oxygen ions of the TiO_2 lattice. Adsorption of copper ions on the anatase surface results in the formation of two types of Cu^{2+} ions in different coordination localized on two types of Lewis acid sites on the surface of TiO_2 [10,11]. The application of XRD and XPS in combination with TPR with H_2 [12] made it possible to determine the concentration of Cu^{2+} ions stabilized on the anatase surface and suggest their possible structure. According to TPR data obtained in that study, there are two types of Cu^{2+} ions with significantly different reducibility on the anatase surface. The high-temperature peak was ascribed to the CuO phase, while the low-temperature one was related to the interaction of copper ions with the support. A similar treatment of the TPR spectra of a Cu–Ti–O system is reported in [13]. However, there are significantly different results. For example, three peaks in the TPR spectrum have been observed in [14], and two low-temperature peaks were ascribed to copper ions with different interaction with the anatase surface. In [15], it has been shown that the type of the TPR spectrum depends on the type of TiO_2 used in the study. Unfortunately, in the literature there are practically no reports on systematic investigation of the effect of the catalyst preparation method and support structure on the state of Cu^{2+} ions stabilized on the anatase surface. There structures are not discussed, and no direct correlation between the state of the active component and catalytic properties of Cu–Ti–O catalysts is reported.

In the present paper results of the study of a series of Cu–Ti–O catalysts by various physicochemical methods are reported, and the effect of the structure of the support surface, the catalyst preparation method and surface copper concentration on the states of Cu^{2+} ions is discussed. The investigation of their catalytic activity in CH_4 oxidation and NO SCR with ammonia made it possible to discriminate the forms of copper most active in these reactions.

2. Experimental

2.1. Catalyst preparation

Titanium oxide synthesized in the laboratory by precipitation from $TiCl_4$ ('ultra pure' grade) with ammonia solution at pH = 7 and $T = 70°C$, as described in [8], was used for synthesis of the catalysts. TiO_2 had been calcined in the air at 500°C for 4 h. No impurity Cl^- ions were detected in the TiO_2 sample. Its specific surface area was $74\,m^2\,g^{-1}$ with the average pore radius of 221 Å. The XRD analysis confirmed the anatase structure of the sample. The average size of TiO_2 crystallites was 210–230 Å.

The catalysts were prepared by incipient wetness impregnation of TiO_2 with a $Cu(NO_3)_2 \cdot 3H_2O$ ('pure for analysis' grade) solution. The copper content was varied from 2.4 to 12 wt.%. In the text, the samples will be denoted as I(n) where n is the copper concentration. One catalyst was synthesized by equilibrium Cu^{2+} adsorption on the TiO_2 surface from 0.47 M copper tetraammoniate solution for 3 days according to [10,11]. After the adsorption procedure, the sample was carefully washed with distilled water. This catalyst will be denoted as A(1.52) where 1.52 is the copper content in this catalyst (in wt.%). All the samples were dried with fast stirring under an IR lamp at 110°C and calcined in the air at 500°C for 4 h.

Copper oxide was prepared by calcination of the initial copper nitrate in the air at 500°C for 4 h.

2.2. Catalysts characterization

IR spectra of CO adsorbed on the TiO_2 sample were recorded on a UR-20 (Carl Zeiss Jena) spectrometer. Prior to the adsorption, the samples pressed into pellets with the density $8–12\,mg\,cm^{-2}$ were successively calcined at 500°C in oxygen for 1 h, under vacuum for 30 min and again in oxygen for 30 min. Then, they were cooled in oxygen to 300°C and evacuated for several minutes to 10^{-4} Torr. CO was adsorbed at liquid nitrogen temperature in small portions to the total pressure 1–5 Torr. The concentration of adsorbed CO was calculated from the integral intensity of the absorption bands using extinction coefficients $1.5\,cm\,\mu mol^{-1}$ for the 2180–$2190\,cm^{-1}$ band and $1.1\,cm\,\mu mol^{-1}$ for the 2195–$2200\,cm^{-1}$ band [16].

XRD spectra were recorded on an HZG-4C diffractometer (Freiberger Prazisionmechanik) with monochromatic Cu Kα irradiation. The mean crystallite sizes of TiO_2 and CuO particles were determined from XRD line broadening measurements using Scherrer equation [17]. The reflex at $d = 1.89$ Å corresponding to (200) anatase face (No. 21-1272, JCPDS-ICDD) was used for determination of the TiO_2 average crystallite size. The average sizes of CuO crystals were determined from the reflex at $d = 2.52$ Å corresponding to (−1 1 1) CuO face (No. 5-661, JCPDS-ICDD). Quantitative X-ray diffraction data were obtained by comparing CuO (−1 1 1) intensity measured for catalyst samples and for physical mixtures of pure CuO and TiO_2.

UV–VIS diffuse reflectance spectra were recorded in the air at room temperature on a Specord-M40 spectrometer (Carl Zeiss Jena) with an attachment for diffuse reflectance measurements. The spectra were recorded with compensation of the absorption of initial TiO_2.

EXAFS spectra of the K-edge of copper absorption were recorded on an EXAFS spectrometer of Siberian Synchrotron Irradiation Center using a transmission technique with the electron energy 2 GeV and average stored current during the measurements 70 mA. A cut-off monocrystal Si (1 1 1) was used as a monochromator. Due to the soft X-ray energy spectrum of VEPP-3 beam line the intensity of the third harmonic (at 27 keV) is negligible. Therefore, suppression of harmonics is not needed. Ionization chambers filled with argon were used for registration of the X-ray radiation. The samples were prepared in the form of pellets to obtain the absorption jump at the Cu-K edge 0.4–0.8. The oscillating component was discriminated according to a standard procedure [18]. Determination of the radial distribution of atoms (RDA) function and the curve fitting procedure were performed for $k^3\chi(k)$ in the range of wave numbers 4.0–12.5 $Å^{-1}$ with the use of EXCURV-92 computer program [19]. Crystalline copper oxide CuO with known structure [20] was used as a model compound. The quality of simulation was estimated from discrepancy factors between the experimental and simulation data (*R*-factor).

Before TPR experiments the samples were heated in oxygen at 500°C for 30 min and cooled in oxygen to room temperature. Then, oxygen was changed for argon, and argon changed for the feed (10 vol.% H_2 in Ar), successively. The feed flow rate was 40 ml min^{-1}. A gradient-free heater with forced air circulation was used in the TPR experiments. The rate of heating from room temperature to 600°C was 10°C min^{-1}. During the experiment H_2O was frozen out at −80°C. The hydrogen concentration was determined with the use of thermal conductivity detector. Parameter P defined in [21] as $P = \beta S_0/FC_0$ (β is the heating rate, °C min^{-1}, S_0 the amount of sample, mol, F the total flow rate, ml min^{-1}, and C_0 the hydrogen concentration in the feed, mol ml^{-1}) was < 20. According to [21], such P value is optimal for TPR experiments. A constant level of hydrogen absorption was maintained by changing the weight of the sample (0.25–0.5 mm particle size) from 20 to 400 mg. The catalyst was diluted to constant volume (1 ml) with quartz glass (0.4–0.7 mm particle size) for evening the thermal exchange conditions along the catalyst bed.

ESR spectra were registered in *x*-range at room temperature without pretreatment of the samples on an ERS-221 spectrometer.

The copper concentration in the samples was determined by atomic absorption spectroscopy. The content of chloride ions in the TiO_2 sample was determined by X-ray fluorescence analysis using a VRA-20 device with W-anode.

The TiO_2 porous structure was studied by mercury porometry in the pressure range of 0.13–200.00 MPa. Specific surface area of the samples was determined by argon thermal desorption.

2.3. Catalytic activity

The catalytic activity of the Cu–Ti–O samples in NO SCR with ammonia was studied by a flow method at 150°C and the following feed composition: 400 ppm NO, 550 ppm NH_3, 0.5 vol.% O_2 in He. The contact time was 0.033 s. The activity of the catalysts was characterized as the NO conversion. Before the catalytic activity tests, the catalysts with the granule size 0.25–0.5 mm were activated in the initial gas mixture at 400°C for 1 h. The NO concentration was measured by a chemiluminescent gas analyzer.

The catalytic activity of the Cu–Ti–O samples in the CH_4 oxidation was studied in a flow ideal-mix-

ing reactor with vibrofluidized catalyst bed at 500°C with the following feed composition: 1.5 vol.% CH_4, 10 vol.% O_2 in He. The contact time was 0.16 s. Before the tests, the catalysts with the granule size 0.25–0.5 mm were activated by oxygen at 500°C for 1 h. The concentrations of CH_4 and CO_2 were determined by a gas chromatographic method. The activity of the catalysts was characterized by the first-order rate constant.

3. Results

3.1. TiO_2 study

Fig. 1 presents the IR spectra of CO adsorbed on the surface TiO_2 at different surface coverages with carbon monoxide. At the lowest concentration of adsorbed CO (0.5 molcules nm^{-2}) the spectrum can be described by two peaks with maximums at 2203 and 2220 cm^{-1}, with the area of the second peak being relatively low (16%). As the amount of adsorbed CO grows, the absorption band is shifted to lower frequency by 15 cm^{-1}. According to [22], such shift of the absorption band maximum with growing coverage of the anatase surface with CO indicates the presence of adjacent Lewis acid sites on the TiO_2 surface. The spectrum corresponding to the maximum concentration of adsorbed CO can be resolved into three Gauss lines with maximums at 2176, 2188 and 2200 cm^{-1} (Fig. 1a). The absorption band at 2200 cm^{-1} corresponds to the strongest α Lewis sites. Such sites are four-coordinated Ti^{4+} ions located primarily on (1 1 0), (1 1 1) and (1 1 3) faces of the anatase surface [23–25]. The concentration of these sites is about 0.3 sites nm^{-2}. The absorption band at 2188 cm^{-1} corresponds to weaker β Lewis sites. They are formed by five-coordinated Ti^{4+} ions forming long chains, primarily, on (1 0 1), (0 1 1) and (0 0 1) faces [23–25]. Their concentration is 4.7 sites nm^{-2}. The observation of the band at 2176 cm^{-1} seems to indicate the presence of weaker Lewis sites with the concentration of 0.6 sites nm^{-2}. This absorption band has been observed in [22]. In [25] it was supposed to correspond to surface Ti^{4+} bonded with hydroxyl groups.

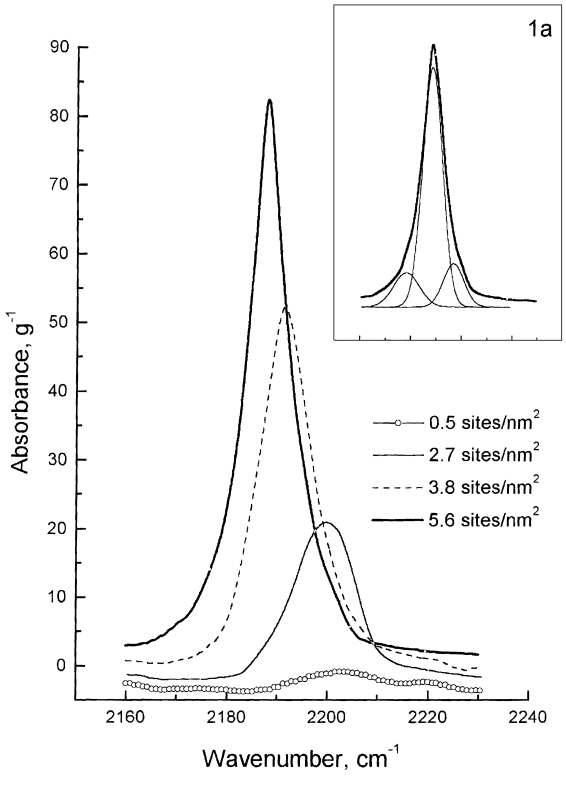

Fig. 1. IR spectra of adsorbed CO with different surface coverage of TiO_2. 1a —the spectrum deconvolution to constituents for CO coverage 5.6 sites nm^{-2}.

Table 1
Main characteristics of prepared Cu–Ti–O catalysts

Sample	S_{BET}, $m^2\,g^{-1}$	Cu concentration[a]		% of monolayer[c]
		wt.%	ions nm^{-2}[b]	
A(1.52)	74	1.52	2.0	28
I(2.4)	61	2.41	3.2	45
I(4)	63	4.05	5.4	76
I(5.6)	59	5.72	7.8	110
I(8)	59	8.31	11.8	166
I(12)	47	12.25	18.4	259

[a] Copper content according to chemical analysis.
[b] Calculated in assumption of monolayer distribution of copper ions on the surface.
[c] Monolayer concentration was taken equal to 7.1 ions nm^{-2}, as in [1].

3.2. Investigation of Cu–Ti–O catalysts

Table 1 presents the main characteristics of studied copper–titanium oxide catalysts.

3.2.1. XRD

CuO phase was not observed in sample A(1.52). Table 2 presents the dependence of the CuO content

Table 2
XRD data for Cu–Ti–O samples

Sample	CuO content		Mean crystallite size of CuO particles, Å
	wt.% Cu	ions nm^{-2}	
I(2.4)	0.4	0.4	400
I(4)	0.5	0.7	450
I(5.6)	1.2	1.6	450
I(8)	2.3	3.3	310
I(12)	3.8	5.7	310
CuO	–	–	460

according to X-ray data on the copper concentration for catalysts prepared by impregnation. In samples I(2.4) and I(4) the CuO content is very low. Further increase of the copper concentration in the catalysts leads to the growth of the CuO content. The maximum CuO content corresponding to about 30% of introduced copper is observed in sample I(12). Note that this sample has significantly lower surface area (Table 1). The mean crystallite size of the CuO particles is also presented in Table 2. One can see that the CuO dispersion in samples with low copper contents (2.4–5.6%) is comparable to that of bulk CuO prepared from copper nitrate. Further increase of the copper concentration to 12% results in a significant decrease of the CuO average crystallite size (Table 2).

3.2.2. UV–VIS diffuse reflectance spectroscopy

An absorption bands at 12,200 cm^{-1} and a charge transfer band at 25,000 cm^{-1} are observed in diffuse reflectance spectra of samples with low copper contents A(1.52) and I(2.4) (Fig. 2). According to [26], the absorption band at 12,200 cm^{-1} can be ascribed to d–d transitions in Cu^{2+} ions in the octahedral coordination with elongated axial distances Cu–O, while the band at 25,000 cm^{-1} corresponds to the charge transfer Cu–O–Ti [9,27]. Note that TiO_2 has

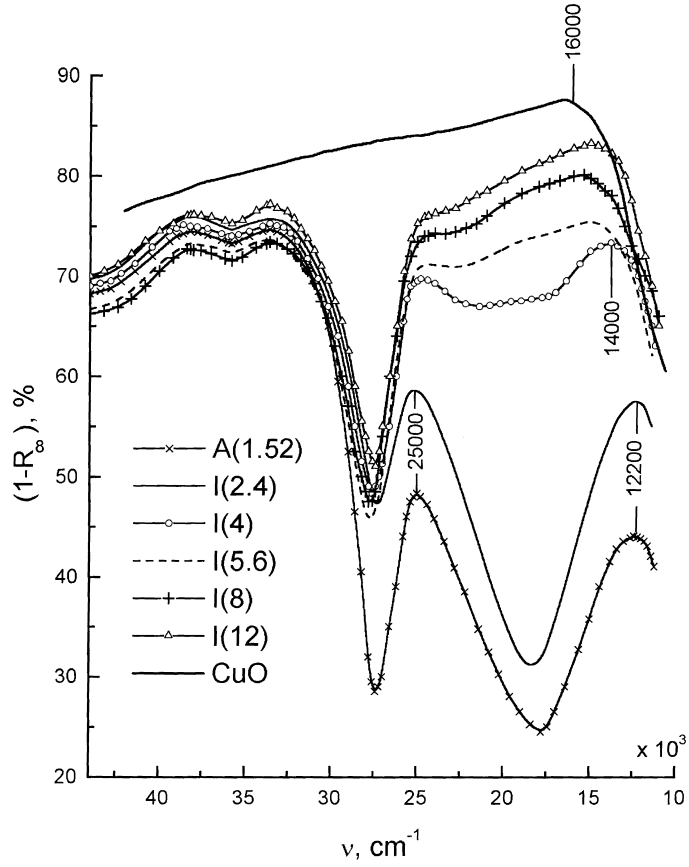

Fig. 2. UV–VIS diffuse reflectance spectra of Cu–Ti–O samples and CuO.

the adsorption edge about 27,000 cm^{-1}. The interaction of copper ions with oxygen anions of anatase lattice seems to lead to change of Ti–O bond energy and to appearance of the adsorption band at 25,000 cm^{-1}. An increase of non-selective absorption in the range of 26,000–12,000 cm^{-1} is observed in the spectrum of sample I(4), while the 12,200 cm^{-1} band is shifted to 14,000 cm^{-1} (Fig. 2). The spectra of samples I(5.6), I(8) and I(12) characterized by even more intensive non-selective absorption are very similar and not much different from the spectrum of bulk CuO (Fig. 2).

An increase of the copper content on the TiO_2 surface seems to result in the copper aggregation and, then, growth of the linear size of oxide clusters. As a result, the axial Cu–O bonds weaken while the in-plane Cu–O bonds strengthen. This leads to a blue shift of d–d transitions. In the limiting case, the structure of bulk CuO can be considered both as a six-coordinated complex with long axial bonds [28] or as a square complex where axial bonds are not taken into account. The appearance of oxide clusters and relatively large CuO particles, in turn, leads to the appearance of non-selective absorption, which is typical for bulk CuO.

3.2.3. ESR

ESR spectra of all catalysts prepared by impregnation are similar with a singlet at $g = 2.14$ ($\Delta H =$ 250 G). A weakly resolved hyperfine structure is observed only in the spectrum of sample I(2.4) with the concentration of paramagnetic Cu^{2+} ions corresponding to 10.4% of the total copper content or 0.3 ions nm^{-2}. Further increase of the copper concentration leads to a sharp drop of the ESR spectrum intensity. Starting from the copper content of 5.6%, the concentration of paramagnetic Cu^{2+} ions does not change and stays at 0.13–0.14% (wt.).

3.2.4. EXAFS

In the curves of radial atom distribution (RDA) obtained by EXAFS (Fig. 3), only distances shorter than 5 Å were analyzed due to a significant contribution of multiple scattering for longer distances.

Table 3 presents interatomic distances and coordination numbers calculated from EXAFS data. Besides the first coordination sphere, only distances Cu–Cu or Cu–Ti were taken into account during the processing of the experimental data. Such constraint was used due to the fact that EXAFS spectroscopy has a limitation on the number of independent variables (13) for the particular experimental data [30], for that Debye–Waller factors were fixed on 0.008 $Å^2$ during fitting procedure for all coordination spheres excluding first Cu–O sphere. Upon fitting for each sphere R and N were varied, with E_0 being constant. Furthermore, the account of scattering only on cations describes the experimental data fairly well. This can be seen from the values of discrepancy factor between the experimental and simulation data (R-factor) presented in Table 3.

According to the data presented in Table 3, the interatomic distances and coordination numbers in samples with the copper content above 2.4% are close to those of bulk CuO. Certain discrepancies of the coordination numbers may be due to the presence of regions with significantly overlapping peaks. In this case, random mismatches both to higher and to lower values can be observed due to the interference of the peaks and their correlation.

Main differences from the spectra of CuO are observed for samples with low copper contents A(1.52) and I(2.4). In these samples the nearest copper-metal distance is by 0.06 Å longer than the Cu–Cu distance in CuO equal to 2.87 Å (Table 3). As the first Ti–Ti distance in anatase is equal to 3.04 Å and a number of coordination spheres corresponding to the CuO structure are not observed in the radial atomic distribution curves (Table 3), this distance might correspond to a Cu–Ti distance. The next distance observed for sample A(1.52) is equal to 3.82 Å. This distance is equal for CuO and TiO_2 structures (Table 3). However, due to the lack of intermediate distances corresponding to the structure of CuO clusters, it is natural to ascribe this distance to copper ions coordinated in the anatase structure. The distance 3.6 Å observed for sample I(2.4) is not present in the structures of copper oxide and anatase. The distances 4.76 and 4.89 Å are close to the third Ti–Ti distance in TiO_2 (Table 3), while the distance 3.4 Å corresponds to the CuO structure.

A peak at distances exceeding 5 Å is observed in the RDA curve of bulk CuO (Fig. 3). The appearance of this peak in the RDA curves of catalysts indicates the formation of CuO clusters with more

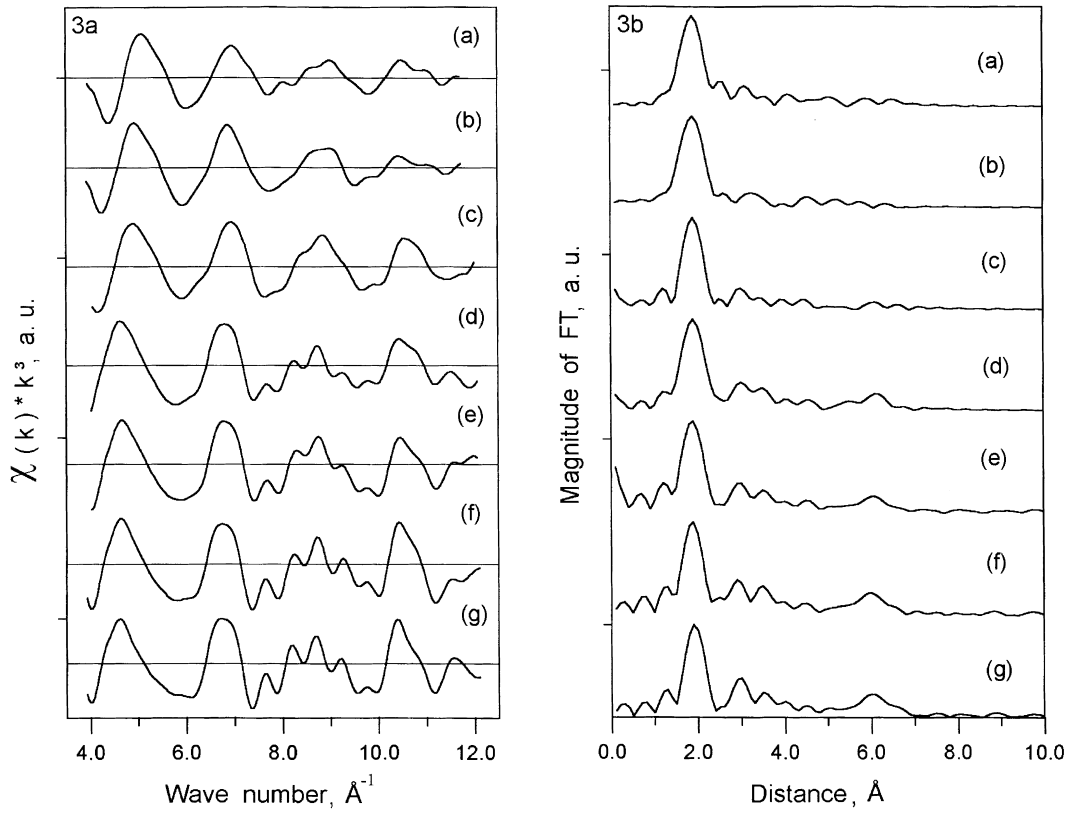

Fig. 3. Experimental curves $k^3\chi(k)$ (3a) and functions of RDA (3b) calculated for cooper local surrounding of the Cu–Ti–O samples: (a) A(1.52); (b) I(2.4); (c) I(4); (d) I(5.6); (e) I(8); (f) I(12); (g) bulk CuO.

than 4–6 atoms. The intensity of this peak depends on the size of the clusters and the fraction of copper present in the form of such clusters. Based on the analysis RDA curves, it is possible to claim that clusters with more than 4–6 copper atoms are not observed for samples A(1.52) and I(2.4). They ap-

Table 3
EXAFS data for Cu–Ti–O catalysts and bulk CuO

	A(1.52)		I(2.4)		I(4)		I(5.6)		I(8)		I(12)		CuO		TiO_2[a]	
	R[b]	N[c]	R	N	R	N	R	N	R	N	R	N	R	N	R[d]	N
Cu–O	1.94	3.2	1.95	3.5	1.94	3.6	1.93	3.7	1.92	4.1	1.93	4.0	1.94	3.5	1.94	4
Cu–M[1]	2.93	1.8	2.94	1.2	2.88	2.7	2.86	3.3	2.86	3.6	2.87	4.8	2.87	3.6	3.04	4
Cu–M[2]					3.05	4.0	3.05	4.0	3.08	4.0	3.09	7.0	3.00	3.0	3.79	4
Cu–M[3]					3.12	2.0	3.14	2.0	3.18	2.0	3.12	2.0	3.10	2.0	4.85	8
Cu–M[4]			3.40	1.2	3.37	2.1	3.37	3.0	3.38	3.6	3.39	4.2	3.43	2.1		
Cu–M[5]	3.82	1.5	3.60	1.0	3.70	0.5	3.83	1.0	3.84	1.0	3.86	1.0	3.81	2.0		
Cu–M[6]			4.76	7.0					4.67	0.3	4.67	0.3	4.67	5		
Cu–M[7]			4.89	0.5												
R-factor, %	19.1		19.9		20.3		18.1		19.5		22.6		19.0			

[a] XRD data for TiO_2 with anatase structure [29].
[b] R is distance from a copper atom to an oxygen atom or a cation (Cu or Ti) in Å.
[c] N is the coordination number.
[d] R is distance from a titanium atom to an oxygen atom or a titanium cation in Å.

pear only in sample I(4). At higher copper contents the RDA curves of the catalysts at distances exceeding 5 Å are similar to that of CuO. One should bear in mind that using only EXAFS data it is impossible to distinguish two limiting cases of copper organization: when about one half of copper is in the form of CuO phase, the rest being in clusters with the number of atoms less than four to six (1); and when most copper is in small clusters containing four to nine copper atoms (2).

3.2.5. TPR

The copper reduction in Cu–Ti–O catalysts studied was as high as 70–80%. Meanwhile, the TiO_2 reduction degree did not exceed 0.3% with hydrogen absorption observed only at the high-temperature edge of the temperature range studied. During the processing of TPR spectra of Cu–Ti–O samples, the background related to the reduction of TiO_2 was subtracted.

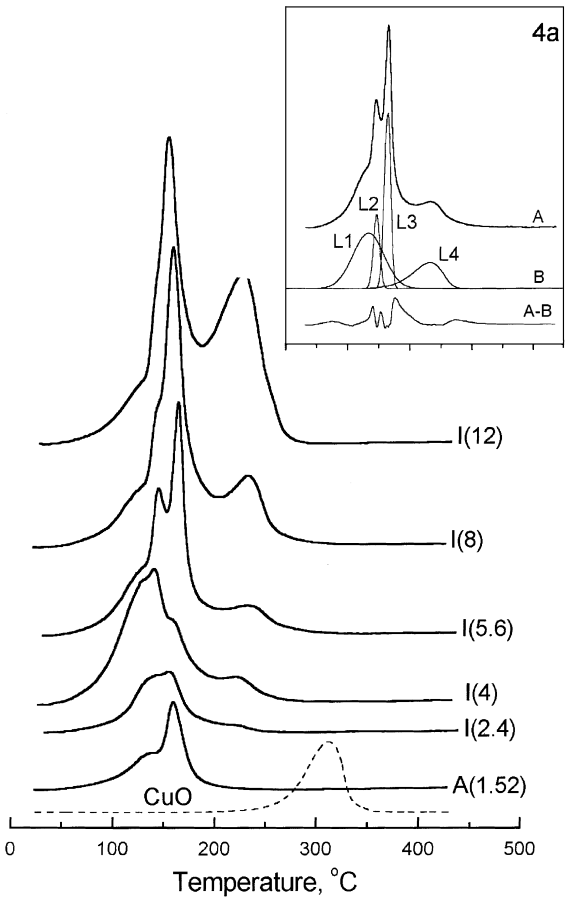

Fig. 4. TPR spectra of Cu–Ti–O samples. 4a — example of a spectrum deconvolution to constituents.

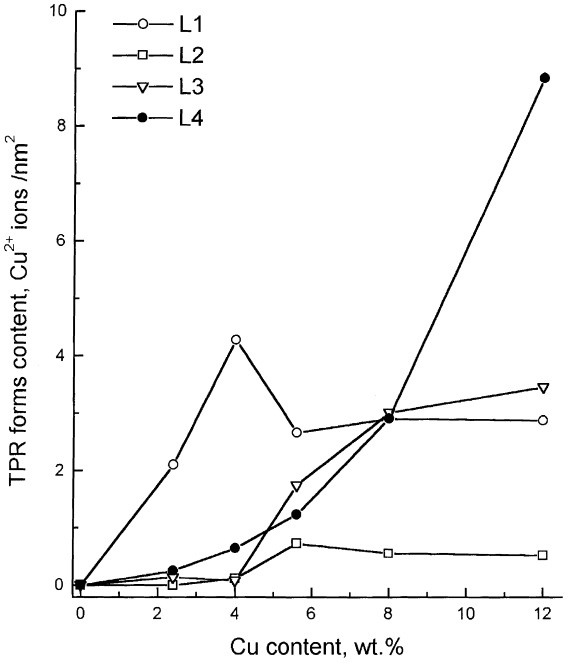

Fig. 5. Dependence of concentration of forms distinguished in the TPR spectrum on the copper content.

Fig. 4 presents TPR spectra of the catalysts studied and CuO sample prepared from copper nitrate. The reduction of bulk CuO takes place at much higher temperatures than that of the catalysts, and only one peak similar to the one reported in [31] is observed in the TPR spectrum of the catalysts. The analysis of complex TPR spectra of Cu–Ti–O samples has shown that TPR spectra of all catalysts prepared by impregnation can be described by a set of four peaks (L1–L4): L1-135°C, L2-140°C, L3-160°C and L4-230°C. Peaks L1 and L2 have almost the same maximums but very different linewidths. As an example, the deconvolution of the TPR spectra of sample I(5.6) is shown in Fig. 4a. The dynamics of changes in the integral intensity of individual peaks as a function of the copper concentration is presented in Fig. 5 as the number of Cu^{2+} ions nm^{-2}. At the copper content of 2.4%, peak L1 dominates in the TPR spectrum with a minor contribution of peaks

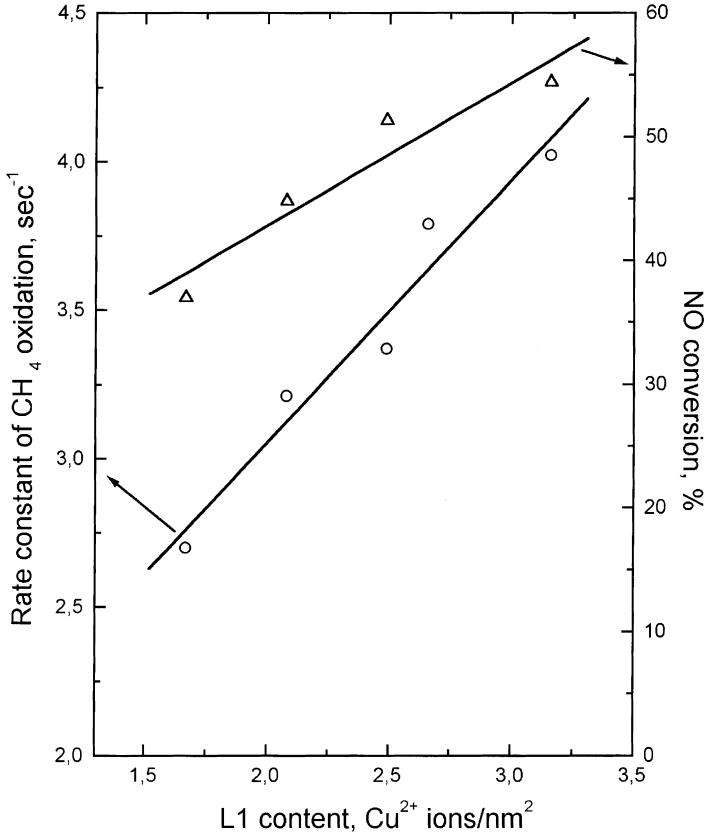

Fig. 6. Activity of Cu–Ti–O catalysts in CH_4 oxidation and NO SCR with ammonia as a function of the content of form L1.

L3 and L4. An increase of the copper content to 4% results in a significant growth of the intensity of peak L1 and appearance of a very weak peak L2, the intensity of peak L3 remaining constant. Note that the intensity of peak L1 reaches its maximum value equal to 4.3 ions nm^{-2} at this copper concentration (Fig. 5). Its intensity decreases to 2.9 ions nm^{-2} at the copper content of 5.6% and is no longer changed with subsequent increase of the copper concentration. Parallel to the decrease of the intensity of peak L1 at the copper content of 5.6%, the contributions of peaks L2, L3 and L4 grow. At the copper content of 8%, peaks L2 and L3 reach their maximum values of 0.6 and 3.4 ions nm^{-2}, respectively. An increase of the copper concentration to 12% leads to a significant growth of the contribution of peak L4 (Figs. 4 and 5). Only two peaks L1 (1.6 ions nm^{-2}) and L3 (0.4 ions nm^{-2}) are observed in the TPR spectrum of sample A(1.52) prepared by equilibrium adsorption (Fig. 4).

3.3. Catalytic activity

The investigation of the catalytic activity of copper–titanium oxide catalysts in deep oxidation of CH_4 and NO SCR with ammonia has shown a relationship between the activity of the catalysts in the above reactions and the content of form L1. The catalytic activity grows with the increase of the concentration of Cu^{2+} ions in form L1 (Fig. 6).

4. Discussion

According to the TPR data, there are four forms of Cu^{2+} stabilization in the catalysts studied (L1–

L4). The dependence of the concentration of high-temperature form L4 on the copper content (Fig. 5) is similar to that of the CuO phase determined from the XRD data (Table 2). Therefore, peak L4 must be related to the reduction of bulk CuO. The temperature corresponding to the maximum of the peak of CuO reduction in Cu–Ti–O samples is lower than the reduction temperature of CuO sample prepared from copper nitrate. Apparently, smaller CuO particles are formed on the surface of the catalysts, and this results in a decrease of the reduction temperature [15].

The temperatures corresponding to the maximums of peaks L1–L3 practically do not change with the growth of copper content (Fig. 4). Moreover, there are maximum surface concentrations of these forms. A significant growth of the concentration of the CuO phase is observed only when these maximum concentrations are reached (Figs. 4 and 5). This indicates that peaks L1–L3 are related to surface Cu^{2+} compounds. Structural or energetic differences between them leading to different reduction temperatures may be caused by the structure of the support.

Faces (0 0 1), (1 0 1) and (0 1 1) are known to be the main faces on the surface of nanosize TiO_2 supports with the anatase structure [23–25]. It is these faces that are places of localization of β Lewis sites [23–25]. In [12], it has been supposed that chain structures are formed from Cu^{2+} ions on the surface of anatase face (0 0 1) where five of six oxygen anions in the nearest octahedral environment of a copper cation belong to the anatase lattice. However, EXAFS data obtained in this study do not support this hypothesis. In our opinion, the formation of two types of one-dimensional band structures where Cu^{2+} ions occupy crystallographic positions of Ti^{4+} ions (Fig. 7a and b) is most probable for face (0 0 1) since coordination numbers for Cu–O bond no more than

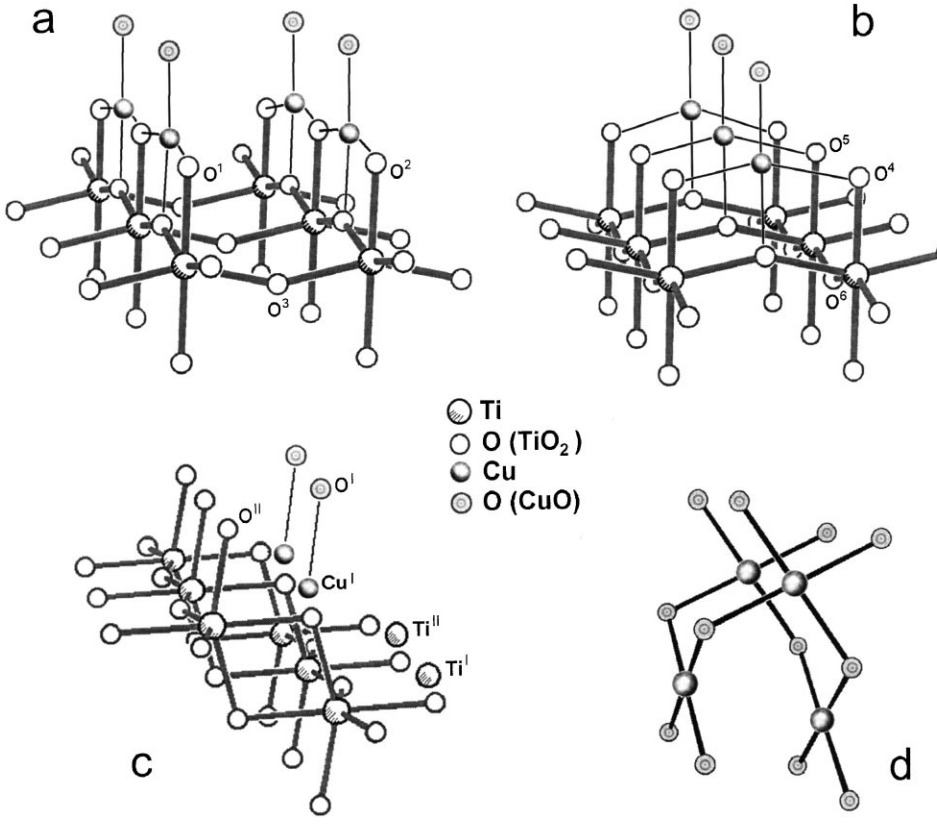

Fig. 7. Possible stabilization structures of Cu^{2+} ions on TiO_2 surface (a, b, c) and structure of a CuO cluster (d).

4. In this case, copper ions are adsorbed on low-coordinated oxygen ions of the anatase surface located near β Lewis acid sites. Judging from structures presented in Fig. 7a and b, it is possible to suppose that different strength of the Cu–Cu bond is due to the fact that in one case (structure A) the Cu–Cu interaction involves x^2-y^2 orbitals (Fig. 7a) where this interaction is strong, while in the other case (structure B) it involves z^2 orbitals (Fig. 7b) where this interaction is weak [26]. Suggested structures are in a good agreement with the EXAFS data. In both discussed structures the nearest Cu–Ti distance corresponds to the distance 2.93 Å observed for sample A(1.52) and distance 2.94 Å observed for sample I(2.4) (Table 3). The distance 3.82 Å corresponds either to the Cu–Cu distance in the chains of both structures or to the Cu–Ti distance typical to Cu^{2+} ions located in node positions of Ti^{4+} ions. The distances 4.76 and 4.89 Å observed for sample I(2.4) (Table 3) are close to the Ti–Ti distance equal to 4.85 Å. Therefore, it can be ascribed to a Cu–Ti distance. According to the EXAFS data, copper ions are four-coordinated in all samples. Meanwhile, according to the electron spectroscopy data, the coordination of Cu^{2+} ions is close to octahedral in the samples with low copper contents. This octahedron is most symmetric at the lowest concentrations, and its axial stretching grows with the increase of the copper content. This contradiction can be explained by the coordination of water present in the samples at the axial positions. As $Ti–OH_2$ and Ti–O distances are different, the former would not have a significant contribution to the radial distribution curve. As the copper content grows, the mean length of the chains of copper ions increases as well. This results in strengthening of the interaction between adjacent copper ions and weakening of $Ti–OH_2$ bonds. Note that water coordination at the axial positions is more natural for structure A. In structure B the existence of two copper ions in octahedral coordination at the distance of 3.8 Å is possible only in the case of a strong distortion of the structure.

Faces (1 0 1) and (0 1 1) are known from the anatase crystal symmetry [32] to be identical and contain many extended step defects. In contrast to face (0 0 1), the structure of these faces does not allow the formation of a structure where Cu^{2+} ions in four-coordinated oxygen environment occupy crystallographic positions of Ti^{4+} ions. However, Cu^{2+} ions can be adsorbed on the surface of these faces between low-coordinated oxygen anions, which are also located near β Lewis acid sites. This would lead to the formation of structure C (Fig. 7c). The existence of such structures does not contradict the EXAFS data. For instance, the distance 3.4 Å in sample I(2.4) (Table 3) can be ascribed to the distance $Cu^{I}–Ti^{I}$ (Fig. 7c), while the distance 4.89 Å (Table 3) corresponds to $Cu^{I}–Ti^{II}$ (Fig. 7c). The distance 2.94 Å (Table 3) is in a good agreement with the nearest distance Cu–Ti. Suggested structure is less energetically favorable than structures A and B because here one of the equatorial oxygen atoms is coordinately saturated. It is natural to suppose that the coordination of Cu^{2+} ions shown in Fig. 7c is not rigid and can be changed with an increase of the surface copper concentration.

Let us discuss the attribution of possible surface structures to the forms of reduction of copper ions. A comparison of the concentration of form L1 with the concentrations of Lewis adsorption sites of different strength unambiguously indicates that these sites are not related to the strongest α-sites as the concentration of the latter is significantly lower than that of form L1. Meanwhile, the maximum concentration of form L1 (4.3 ions nm^{-2}) practically matches the concentration of β-sites (4.7 sites nm^{-2}). Form L1 cannot be attributed to isolated Cu^{2+} ions only as its growth with the increase of the copper content from 2.4 to 4% (Fig. 5) is accompanied by a substantial decrease of the intensity of the ESR signal. Moreover, the concentration of paramagnetic Cu^{2+} ions determined by ESR ($\sim 0.2–0.3$ ions nm^{-2}) is significantly lower than the concentration of form L1. Therefore, Cu^{2+} ions in different structures A, B and C (Fig. 7a–c) can be attributed to this reduction form. This is true both for isolated Cu^{2+} ions and ions organized in chains of variable length. The large width of peak L1 in the TPR spectrum seems to indicate a great variety of copper states. Form L1 prevails in the samples with low copper concentration, and its maximum content is observed for sample I(4) with the surface copper concentration 5.4 ions nm^{-2} (Table 1).

According to EXAFS, in sample A(1.52) there are no distances typical to structure C (Fig. 7c) located on faces (1 0 1) and (0 1 1). This may be explained by

a number of reasons. First, copper was deposited on the surface of sample A(1.52) from a basic solution (pH = 11) in contrast to catalysts prepared by impregnation where the copper nitrate solution was acidic (pH = 3–4). Furthermore, NH_4^+ ions and NH_3 molecules present in the solution may block surface sites where copper ions are stabilized. Second, the preparation of sample A(1.52) was performed under equilibrium conditions leading to the formation of the most energetically favorable states of Cu^{2+} ions.

Surface forms of Cu^{2+} ions accounting for narrow reduction peaks L2 and L3 in TPR curves (Fig. 4) may be attributed to two different types of oxide clusters with the structure similar to CuO. Such attribution is favored by the dynamics of changes in the concentration of TPR forms of Cu^{2+} ions with the growth of surface copper concentration. At low copper concentrations ($\leq 4\%$) Cu^{2+} ions are stabilized in form L1. When the anatase surface coverage with Cu^{2+} ions increases, some of L1 sites become nucleation centers of form L3. Indeed, noticeable growth of the concentration of form L3 is accompanied by a decrease of the concentration of form L1 by about 35% when Cu concentration increases from 4 to 5.6% (Fig. 5).

The formation of clusters of Cu^{2+} ions can be imagined as follows. The distance O^I–O^{II} (Fig. 7c) is about 2.9 Å. That is close to the distance between two linked oxygen atoms in the CuO structure (Fig. 7d). We believe that a pair of oxygen atoms O^I–O^{II} can be a site of the formation of an oxide cluster with CuO structure bonded with the surface of the support. The size of the oxide cluster seems to be limited by the pore structure of the support. A similar pair can be formed on face (0 0 1) as well if a CuO structural unit is embedded near structure A between O^1, O^2 and O^3 (Fig. 7a) or near structure B between O^4, O^5 and O^6 (Fig. 7b). In this case, the nearest Cu–Cu distance approaches 2.87 Å, which corresponds to the Cu–Cu distance in the CuO structure (Table 3). Note that the formation of such structures is less energetically favorable than the formation of chain structures A and B where the coordination sphere of a Cu^{2+} ion is formed only by low-coordinated oxygen anions of the anatase lattice.

Unfortunately, the study performed did not allow us to distinguish the difference between oxide clusters L2 and L3. Very low concentration of cluster L2 in comparison with that of L3 can be explained by a number of reasons. Either the number of sites where such clusters are formed is very low, or their formation is energetically unfavorable, or there is a limit on their growth (for example, pore size). Form L2 is not observed in the spectrum of sample A(1.52) (Fig. 4), for which the distance typical to structure C located on (1 0 1) and (0 1 1) faces of TiO_2 is not observed. Therefore, one can suppose that oxide cluster L2 is localized on the above faces.

The growth of the contribution of oxide clusters L3 at copper contents above 5.6% (Figs. 4 and 5) makes it possible to explain the decrease of the average crystallite size from 450 to 310 Å observed by XRD (Table 2). The presence of large CuO crystallites in samples I(2.4) and I(4) and absolute mismatch between the pore size of initial TiO_2 and size of CuO crystallites indicates that in this case bulk CuO is localized on the external surface of the support rather than in the TiO_2 pores. Some of the impregnating solution can be moved to the external surface of granules during drying of samples impregnated with copper nitrate, while the following calcination can result in the formation of large CuO crystallites.

The investigation of the nature of the states of Cu^{2+} ions on the surface of Cu–Ti–O catalysts and tests of their catalytic activity in the CH_4 oxidation and NO SCR have shown that chain stabilization forms of Cu^{2+} ions (L1) are most active in these reactions. Redox transformations of Cu^{2+} ions are known to occur on copper-containing catalysts during methane oxidation or NO SCR with ammonia [33–35]. According to the TPR data, copper ions in form L1 are reduced easier than ions in other forms, i.e. they are characterized by an easier electron transfer (Fig. 4). This characteristic seems to be one of the causes of higher catalytic activity of this form of Cu^{2+} ions in the reactions studied. Moreover, Cu^{2+} ions in from L1 have lower coordination numbers (Fig. 7a–c). This can be another reason of their higher reactivity.

5. Conclusion

The application of a wide number of physicochemical methods and purposeful synthesis of sam-

ples made it possible to characterize the state of Cu^{2+} ions in Cu–Ti–O catalysts more comprehensively. Copper ions in different states are present in the samples of Cu–Ti–O studied by us. The state of copper oxide forms on the TiO_2 surface is determined by its structure, the copper concentration and the catalyst preparation method. At low copper concentrations Cu^{2+} ions preferably interact with low-coordinated oxygen atoms of the anatase lattice with the formation of chain structures of variable length with low number of isolated Cu^{2+} ions. The concentration of these forms and the geometry of the nearest oxygen environment of Cu^{2+} ions are determined by the structure of TiO_2 faces. The most energetically favorable structures are formed on face (0 0 1). As the copper concentration grows, some of the surface oxide copper–titania forms become nucleation centers of oxide clusters. The size of the latter seems to be limited by the size of anatase pores. Noticeable growth of bulk CuO phase takes place after completion of the formation of surface-stabilized Cu^{2+} ions and oxide clusters. The ratio of the forms of copper can be changed in favor of more energetically favorable ones by the application of another preparation method — equilibrium adsorption technique. The investigation performed made it possible to make quantitative evaluation of the contents of different copper forms on the anatase surface and show that surface-stabilized chain forms of Cu^{2+} ions are most active in the CH_4 oxidation and NO SCR with ammonia.

Acknowledgements

We would like to thank Dr. G.A. Zenkovets for the TiO_2 preparing, L.D. Shitova for the carrying out IR measurements, I.L. Kraevskaya for performing the analysis of chloride ions, Dr. R.V. Olkhov for help in the analysis of TPR data and Dr. L.T. Tzykoza for helpful discussions.

References

[1] P. Larsson, A. Andersson, L.R. Wallenberg, B. Svensson, J. Catal. 163 (1996) 279.
[2] P. Larsson, A. Andersson, J. Catal. 179 (1998) 72.
[3] O.V. Komova, A.V. Simakov, L.T. Tzykoza, N.N. Sazonova, A.V. Ushakov, G.B. Barannik, Z.R. Ismagilov, React. Kinet. Catal. Lett. 54 (1995) 361.
[4] G. Centi, C. Nigro, S. Perathoner, G. Stella, Catal. Today 17 (1993) 159.
[5] G. Centi, S. Perathoner, B. Kartheuser, B.K. Hodnett, Catal. Today 17 (1993) 103.
[6] G. Centi, S. Perathoner, B. Kartheuser, D. Rohan, B.K. Hodnett, Appl. Catal. 1 (1992) 129.
[7] O.V. Komova, A.V. Simakov, L.T. Tzykoza, N.N. Sazonova, V.A. Ushakov, G.B. Barannik, Z.R. Ismagilov, React. Kinet. Catal. Lett. 54 (1995) 371.
[8] D.V. Tarasova, N.G. Maksimov, L.T. Tsikoza, G.A. Zenkovets, I.P. Olenkova, Izv. Sib. Otd. Akad. Nauk SSSR 7 (1981) 81 (in Russian).
[9] L.Ya. Mostovaya, N.A. Kovalenko, T.S. Petkevich, Yu.G. Egiazarov, J. Appl. Spectrosc. 60 (1994) 487.
[10] M.M. Kantcheva, K. Hajiivanov, A.A. Davydov, A.A. Budneva, Appl. Surf. Sci. 55 (1992) 49.
[11] K. Hajiivanov, D. Klissurski, M.M. Kantcheva, A.A. Davydov, J. Chem. Soc., Faraday Trans. 87 (1991) 907.
[12] B. Xu, L. Dong, Yi Chen, J. Chem. Soc., Faraday Trans. 94 (1998) 1905.
[13] F.S. Delk II, A. Vavere, J. Catal. 85 (1984) 380.
[14] M. del Arco, A. Caballero, P. Malet, V. Rives, J. Catal. 113 (1988) 120.
[15] G.C. Bond, S.N. Namijo, J.S. Wakeman, J. Mol. Catal. 64 (1991) 305.
[16] E.A. Paukshtis, IR Spectroscopy in Heterogeneous Acid–Base Catalysis, Nauka, Novosibirsk, 1992, p. 69 (in Russian).
[17] H.P. Klug, L.E. Alexander, X-Ray Diffraction Procedures for Polycrystalline and Amorphous Materials, 1st Edition, Wiley, New York, 1954.
[18] V.V. Kriventsov, D.I. Kochubey, G.L. Elizarova, L.G. Matvienko, V.N. Parmon, J. Colloid Interface Sci. 215 (1999) 23.
[19] S.J. Gurman, N. Binsted, I. Ross, J. Phys. C 19 (1986) 1845.
[20] S. Asbrink, A. Waskowska, J. Phys. C: Condensed Matter 3 (1991) 8173.
[21] P. Malet, A. Caballero, J. Chem. Soc., Faraday Trans. I 84 (1988) 2369.
[22] A.A. Tsyganenko, L.A. Denisenko, S.M. Zverev, V.N. Filimonov, J. Catal. 94 (1985) 10.
[23] G. Busca, H. Saussey, O. Saur, J.C. Lavalley, V. Lorenzelli, Appl. Catal. 14 (1985) 245.
[24] K.I. Hadjiivanov, D.G. Klissurski, A.A. Davydov, J. Catal. 116 (1989) 498.
[25] K.I. Hadjiivanov, A.A. Davydov, D.G. Klissurski, Kinetika i kataliz 29 (1988) 161.
[26] A.B.P. Lever, Inorganic Electronic Spectroscopy, Elsevier, Amsterdam, 1984, p. 554.
[27] M. del Arco, V. Rives, React. Kinet. Catal. Lett. 31 (1986) 239.
[28] S. Asbrink, L.J. Norrby, Acta Cryst. B 26 (1970) 8.
[29] C.J. Howard, T.M. Sabine, F. Dickson, Acta Cryst. B 47 (1991) 462.

[30] Report on the International Workshop on Standards and Criteria, in: S.S. Hasnain (Ed.), XAFS in X-Ray Absorption Fine Structure, Ellis Horwood, New York, 1991, p. 751.
[31] A.L. Boyce, S.R. Graville, P.A. Sermon, M.S.W. Vong, React. Kinet. Catal. Lett. 44 (1991) 1.
[32] C.J. Howard, T.M. Sabine, F. Dickson, Acta Cryst. B 47 (1991) 462.
[33] W. Liu, M. Flytzani-Stephanopoulos, J. Catal. 153 (1993) 317.
[34] G. Ramis, L. Yi, G. Busca, M. Turco, E. Kotur, R. Willey, J. Catal. 157 (1995) 523.
[35] T. Iizuka, H. Ikeda, S. Okazaki, J. Chem. Soc., Faraday Trans. I 82 (1986) 61.